1.3 ON THE EFFECTS OF HELIUM-DPA INTERACTIONS ON CAVITY EVOLUTION IN TEMPERED MARTENSITIC STEELS AND NANOSTRUCTURED FERRITIC ALLOYS UNDER DUAL ION-BEAM IRRADIATION - G. Robert Odette, Takuya Yamamoto, Yuan Wu, (University of California Santa Barbara), Sosuke Kondo, Akihiko Kimura (Kyoto University)

OBJECTIVE

The objective of this research is to characterize how cavity and other microstructural evolutions in irradiated candidate 9Cr tempered martensitic steels and nanostructured ferritic alloys are influenced by the starting microstructure and irradiation variables, including temperature, displacements per atom (dpa), dpa rate and the helium/dpa (He/dpa) ratio.

SUMMARY

Cavity evolution in normalized and tempered 9Cr martensitic steels (TMS) F82H under Fe^{3+} and He^{+} dual ion beam irradiation (DII) at 500°C was characterized for new dpa and He conditions. The cavity evolution TMS alloy database at 500°C now includes 88 dpa-He-dpa rate DII conditions. The data indicate there may be two swelling trends. This may partly be due to slightly different irradiation flux and/or temperature conditions plus simply natural scatter that is enhanced by local microstructural variations. The fact that swelling under neutron irradiation conditions at low He levels tends to be highly inhomogeneous is well established. The higher swelling rate upper bound data reaches more than ≈ 3% swelling. In the high swelling rate case, the incubation dpa for the onset of void swelling (dpa_i) decrease linearly with increasing He/dpa, and the data can be collapsed on an incubation-adjusted dpa' (= dpa-dpa_i) master trend band. In the low swelling rate case, the incubation dose is ≈ 20 dpa and the post incubation swelling is much more gradual, and approximately linear, with slopes that increase with He/dpa.

BACKGROUND

As reported previously[1-4] we have been carrying out DII studies at 500°C in DuET facility in Kyoto University at various nominal He/dpa and dpa rates (defined at the depth of 600 nm) in TMS and Nanostructured Ferritic Alloys (NFAs). Here we update the DII database and analyze cavity evolution (and swelling) trends in F82H Mod.3 and IEA heats encompassing a very wide range of DII dpa, He and He/dpa. We also compare the behavior of F82H to that in the NFA MA957.

Experimental Procedure

While details of alloys and DII experiments can be found in [2], Table 1 summarizes nominal He and dpa conditions at two reference depth locations encompassed by the current database. The irradiations targeted two nominal doses, three He/dpa and two dpa rate conditions. Taking advantages of the varying spatial distributions of dpa, He and He/dpa as shown Figure 1a for the latest DI14B irradiation, we characterized the microstructures over a very wide range of He-dpa conditions. Figure 1b shows all the available conditions for F82H IEA and Mod.3 in terms of He to dpa rations, where quantitative analyses of microstructure were performed for the series of depth regions in 100nm increments. The conditions shown in Fig.1b represent the average dpa, He and He/dpa in each 100nm section. The dpa are based on SRIM using the Kinchin-Pease with Fe displacement energy of 40 eV [5,6].

RESULTS

Swelling Trends

We have quantitatively characterized the cavity evolution trend as a function of dpa, He and He/dpa in terms of their average size, <d>, number density, N, and volume fractions f. In the previous analysis [1,2], notably <d> and N vary significantly for similar irradiation conditions. This is largely due to the effects of the local microstructure. However, the corresponding variations in f are less. This reflects the fact that variations in the corresponding void $\langle d_v \rangle$ and N_v are also less, and that the total f ≈ f_v. Here we assume separation of voids from bubbles at a (≈ critical) size of 4 nm, corresponding to the dip between the two peaks in the cavity size distributions at various conditions.

Table 1. Irradiation conditions analyzed in this report

Exp ID	Alloys	T (^{o}C)	Nominal Condition (@550-650nm)				Peak He (@1000-1100nm)		
			dpa	He (appm)	He/dpa	dpa/s	dpa	He (appm)	He/dpa
DI10B1	F82H mod.3, MA957	500	26	1210	47	5.0×10^{-4}	45	2100	47
DI10B2			9.9	457	46	5.2×10^{-4}	17	795	46
DI10B3			10	480	47	5.1×10^{-4}	18	840	47
DI13A1	F82H mod.3	500	26	390	15	5.1×10^{-4}	44	670	15
DI12A1	MA957	650	48	2230	47	1.1×10^{-3}	83	3860	47
DI13B1	F82H mod.3, F82H IEA (AT)	500	30	848	29	1.5×10^{-3}	51	1467	29
DI13B1+2	MA957	500	57	1578	28	1.5×10^{-3}	97	2729	28
DI14A1	F82H mod.3, F82H IEA (AT)	500	26	1200	47	1.5×10^{-3}	45	2100	47
DI14A1+2	MA957	500	52	2400	47	1.5×10^{-3}	90	4200	47
DI14B	F82H mod.3, F82H IEA (AT)	500	45	1290	28	8×10^{-4}	79	2230	28

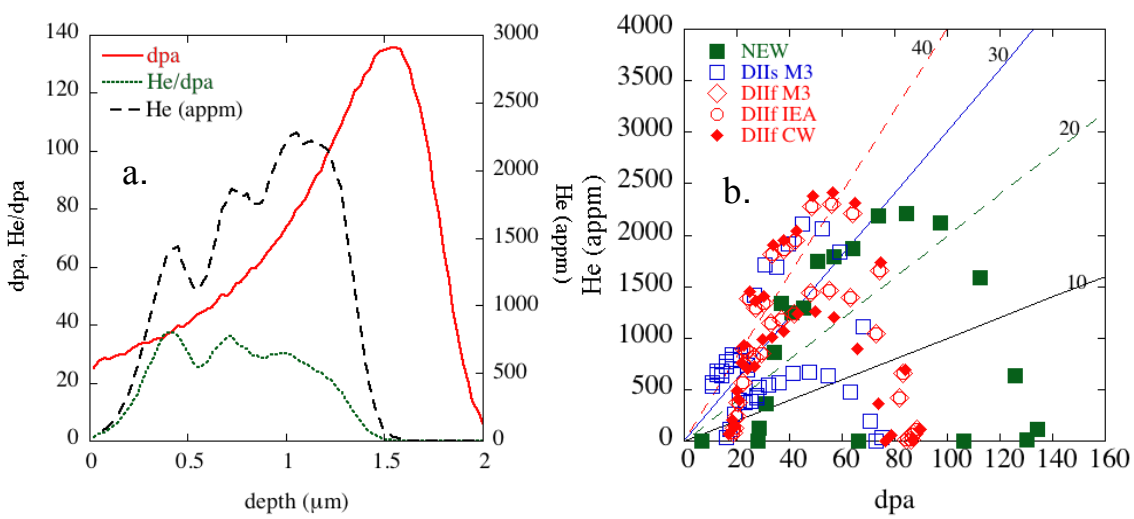

Figure 1. a) The dpa, He (appm) and He/dpa profile of the latest DI14B irradiation, and b) He/dpa - dpa conditions for all the DI runs for TMS materials.

We have updated our database with newly analyzed cavity microstructural data for F82H IEA and Mod.3. To date we have collected data on 88 dpa-He-dpa rate DII conditions for F82H Mod.3 and 48 conditions for F82H IEA. Figure 2 shows a) The number density, b) average diameter, and c) volume fraction of "voids" observed in F82H IEA in dual ion-beam irradiation experiments, as a function of dpa for the groups by nominal He/dpa ratio (SRIM estimated ratio over the analyzed region rounded to the nearest 10s). As shown in Fig.2a the N_v seems to increase monotonously with some scatter for He/dpa of 20 or more, while at lower He/dpa conditions the trend seems to have distinctly 2 groups; one rises sharply around 80 dpa, while the other stays lower until ≈ 130 dpa. The average diameter $<d_g>$ seems less scattered within each He/dpa group. The $<d_g>$ seems to show a steeper initial increase higher He/dpa, followed by gradual decrease. The decrease may be due to continuing nucleation of smaller voids. As a

result of the increasing N_v and $<d_g>$, the f_v show monotonic increases as a single group with significant scatter for He/dpa of 20 or more. However, in one trend for lower He/dpa of 10 the voids continue to remain in the incubation regime, rather than steeply rising at ≈ 80 dpa. These two trends are associated with different DII runs. The results showing higher f_v are from DI14A1, while the lower f_v are from DI14B. The differences in the irradiation conditions are the dpa and He injection rates, which for larger f_v are both about twice as high as that for lower f_v. Higher He and vacancy concentrations may cause higher N_v voids forming on a higher number density of bubbles along with a theoretically smaller critical size for bubble to void conversion. Another factor is a possible difference in irradiation temperature. Temperature was measured using a pyrometer. A rough estimate of the temperature uncertainty is ±25°C.

Figure 3 shows the corresponding a) number density, b) average diameter, and c) volume fraction of "voids" vs. dpa plots for F82H Mod.3. In this case the two groups of trend is even more enhanced, and is observed even at highest He/dpa. The similar split of trends in two alloys that were irradiated side-by-side supports the hypothesis that the differences may be partly related to the irradiation conditions.

Reiterating the data showing faster f_v versus dpa trend in F82H IEA as summarized in a previous report [1], shows that the swelling incubation dose, dpa_i, linearly decreases with He/dpa ratio as shown in Figure 4a. Using the dpa – dpa_i(He/dpa) gives more unified trend of swelling vs. dose in post-incubation swelling trend. Figure 4b shows the f_v trend for F82H IEA irradiated in the DII experiments compared with f_b for bubbles in MA957 (since no voids are present) on thus modified dpa scale (dpa') normalized at He/dpa = 30, which corresponds to dpa_i = 40. Thus we define dpa' = dpa - dpa_i(He/dpa) + 40. The post incubation swelling in the F82H IEA (filled symbols) occurs at a high rate in a scatter band that averages ≈ 0.1%/dpa. In contrast, the f in the NFA are low up to dpa' ≈ 140 dpa. Note that at ultra high helium levels of ≈ 5000 appm most of the nominal f_b is actually occupied within the nano-feature (NF) oxides that are enveloped by the bubble. The volume fraction of the oxides is ≈ 0.5% shown by the horizontal blue box, thus the f_v for the helium itself is estimated to be less than ≈ 0.3%. This result is reasonably consistent with recent measurement of the helium density in small bubbles, which is ≈ 60/nm^3 are r_b = 1.4 nm [7]. These results also confirm approximate predictions of an older equation of state for helium [8] as well as one based on a new atomistic model [9].

As noted previously, these results can be used to estimate the upper bound swelling in the TMS. For example, at He/dpa = 10, dpa_i ≈ 70 and assuming a post incubation rate of ≈ 0.1%/dpa, the estimated swelling at 200 dpa is ≈ 13%. The corresponding bubble swelling in the NFA at 2000 appm helium is estimated to be less than 0.3%. These dual ion data cannot be translated to different temperatures or neutron irradiation conditions. However, Figure 5 also includes data from in-situ helium injection (ISHI) experiments in High Flux Isotope Reactor (HFIR) at fusion relevant conditions as the large crosshatched symbols. Details of the ISHI technique are given elsewhere. Briefly Ni (or B or Li)-bearing implanter layers are used to inject high-energy α particles into an adjacent material that is simultaneously undergoing fast neutron induced displacement damage. Notably, based on an estimated neutron incubation dpa_i ≈ 5dpa at He/dpa≈50, the ISHI swelling data falls in the trend band for the DII. Note that the ISHI database is being extended from 21 to ≈ 35 dpa, that extrapolates to a more significant level of ≈ 1.9% swelling if the lower dose trends persist.

Even in the low swelling rate regime, the void f_v alone exceeds the corresponding bubble f_b in MA957. However, in the low swelling rate case of F82H, f_v is closer to f_b in MA957. The low swelling rate data can be best treated with linear f_v versus dpa fits with a slope M and intercept f_{vo}. These fits have a roughly constant incubation dose of dpa_i ≈ 20 dpa. However, at higher post incubation dpa, the slopes M increase systematically with He/dpa, as M ≈ C[He/dpa]. Fits to both F82H variants slopes yield a C ≈ 0.00018±0.00001. In this case swelling is approximately represented by f_v = 0.00018[He/dpa][dpa - 20]. It is inappropriate to extrapolate this relation. But if this is done for a He/dpa = 10, f_v is 0.36% at 200 dpa does and not reach 1% until ≈ 555 dpa. Finally, it is very important to emphasize that we are not suggesting these estimates that are based on DII irradiations should be considered as being representative of neutron irradiation conditions.

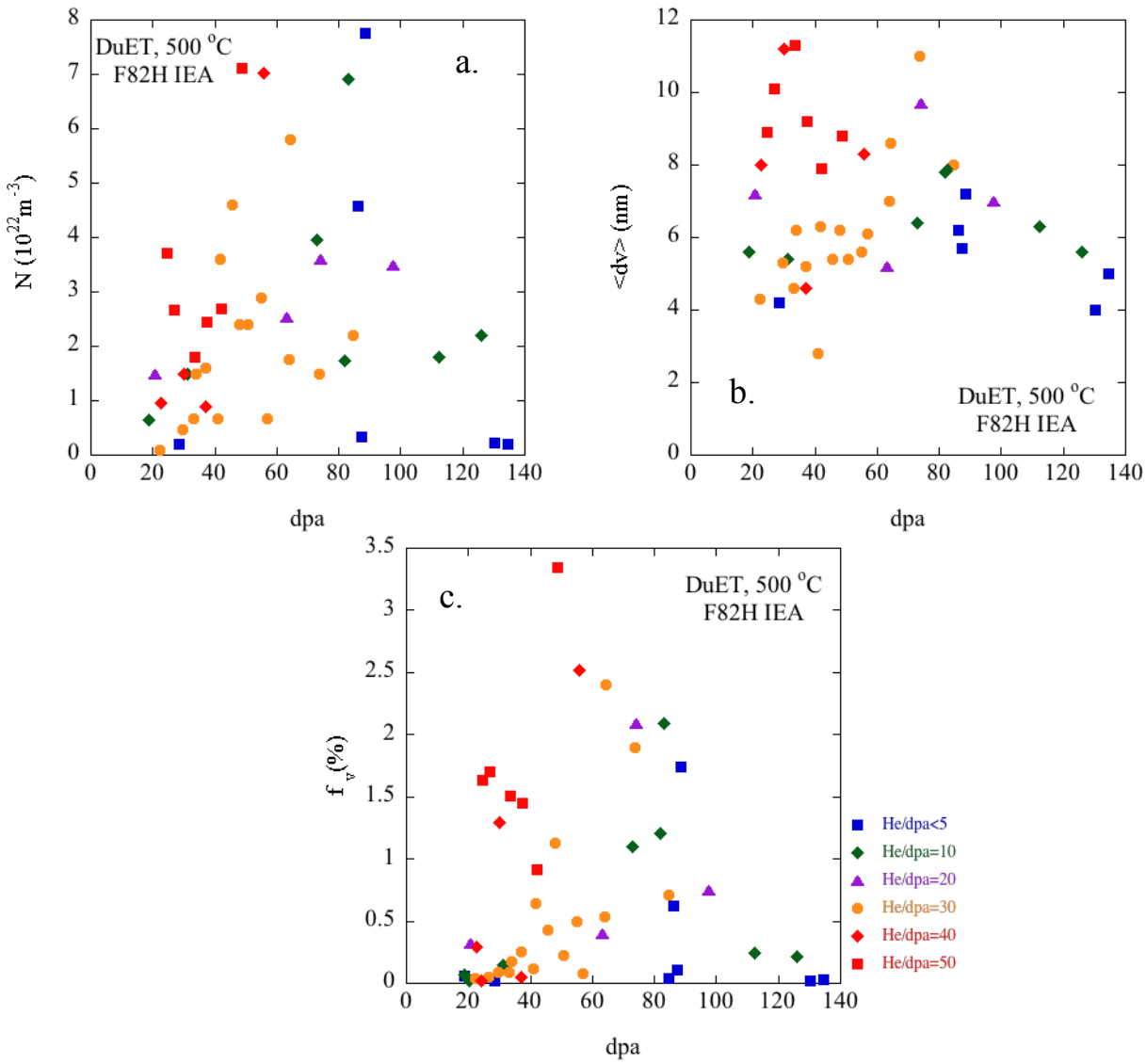

Figure 2. a) The number density, b) average diameter, and c) volume fraction of "voids" observed in F82H IEA in dual ion-beam irradiation experiments, as a function of dpa for the groups by nominal He/dpa ratio.

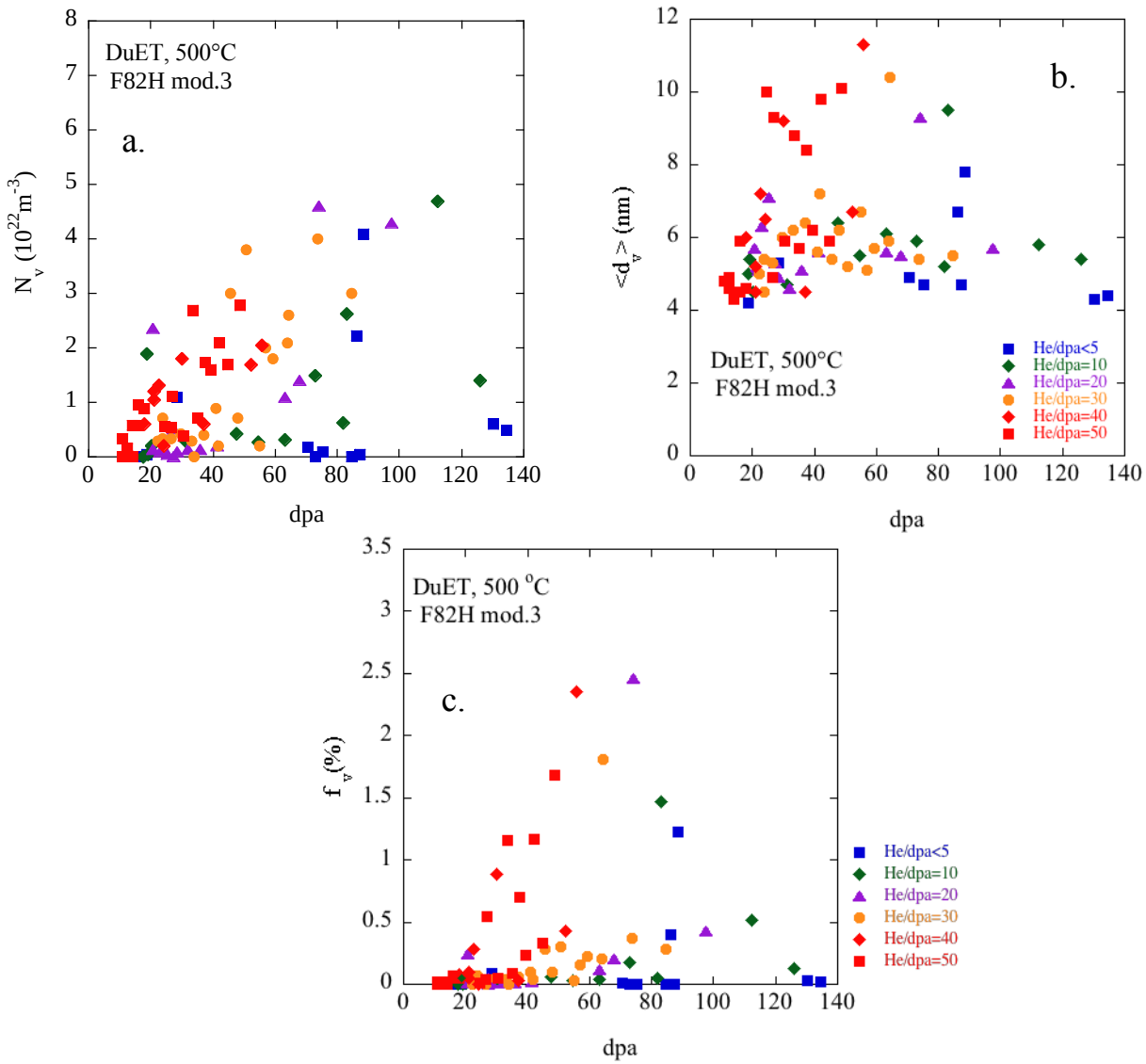

Figure 3. a) The number density, b) average diameter, and c) volume fraction of "voids" observed in F82H Mod.3 in dual ion-beam irradiation experiments, as a function of dpa for the groups by nominal He/dpa ratio.

Summary

Cavity evolutions in normalized and tempered martensitic steel (TMS) F82H under Fe^{3+} and He^{+} dual ion beam irradiations (DII) at 500°C have been characterized over a wide range of dpa, He and He/dpa. The cavity evolution database, that includes 88 dpa-He-dpa rate DII conditions for TMS alloys, shows that the swelling is highly scattered and may manifest two swelling trends. The differences may be partly related to slightly different dpa rates and irradiation temperatures. In the high swelling rate trend case, the incubation dpa_i for the onset of rapid void swelling decreases linearly with increasing He/dpa. In the low swelling rate case the dpa_i are all ≈ 20 and the slopes of f_v versus dpa (>dpa_i)_are the roughly linear and increase, also roughly linearly, with He/dpa. The bubble swelling in the nano-structured ferritic alloy MA957 is smaller compared to the void swelling alone In F82H.

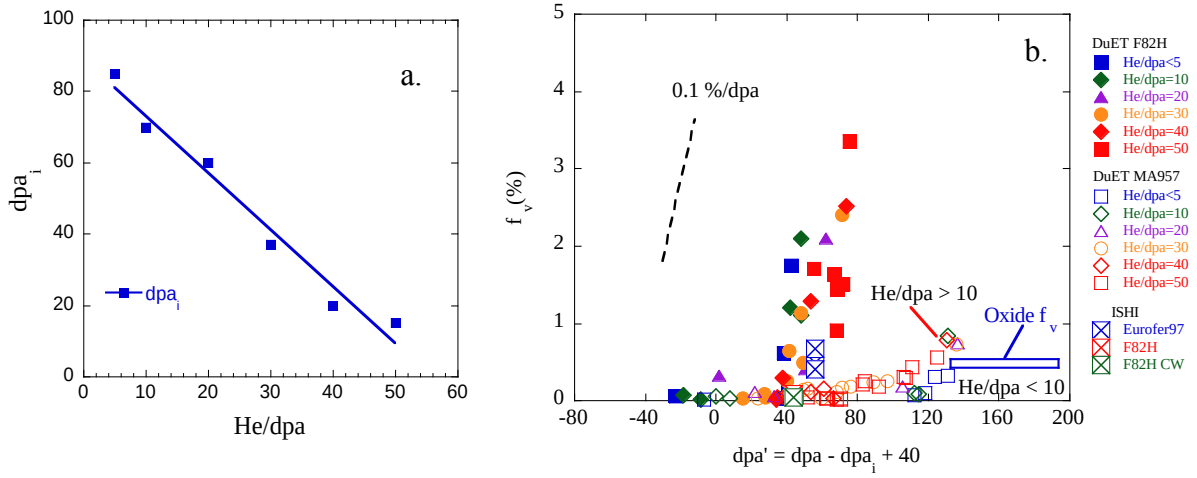

Figure 4. a) swelling incubation dose (dpa_i) versus He/dpa in DII F82H IEA; b) swelling, fv, for F82H IEA compared with NFA, MA957 in DII experiments, as well as with TMS data in in-situ He injection experiments in HFIR.

Acknowledgements

The dual ion-beam irradiations were conducted under the support of the "Joint Research Program on Zero-Emission Energy Research, Institute of Advanced Energy, Kyoto University (ZE26A-16, 25A-19, 24A-13 and 23B-3). The work performed at UCSB was supported by the U. S. Department of Energy, Office of Fusion Energy Sciences, under contract DE-FG03-94ER54275. We acknowledge the contributions of the NSF sponsored UCSB Microstructure and Microanalysis Facility. We are also grateful for generous support of research materials, F82H mod.3 from Dr. K. Shiba, (JAEA, Japan).

References

[1] T. Yamamoto, Y. Wu, G.R. Odette, S. Kondo, A. Kimura, *Fusion Materials Semiannual Report 6/30/2014* DOE/ER-313/56 (2014) 194

[2] T. Yamamoto, Y.Wu, G.R. Odette, K. Yabuuchi, S. Kondo, A. Kimura, J. Nucl. Mater. 449 (2014) 190

[3] T. Yamamoto, Y.Wu, G.R. Odette, S. Kondo, A. Kimura, *Fusion Materials Semiannual Report 6/30/2013* DOE/ER-313/54 (2013) 6.

[4] T. Yamamoto, Y. Wu, G.R. Odette, K. Yabuchi, A. Kimura, *Fusion Materials Semiannual Report 12/31/2010* DOE/ER-313/49 (2011) 1.

[5] ASTM E521-96 (2009), ASTM

[6] R.E. Stoller, M.B. Toloczko, G.S. Was, A.G. Certain, S. Dwaraknath, F.A. Garner, Nuc Instr Mehtods Phys Res B 310 (2013) 75.

[7] Y. Wu, G.R. Odette, T. Yamamoto, J. Ciston, P. Hosemann, Fusion Materials Semiannual, Report 6/30/2013 DOE/ER-0313/54, 2013, pp. 172

[8] R. E. Stoller and G. R. Odette, J. Nucl. Mater. 131 (1985) 118..

[9] R. E. Stoller and Y. N. Osetskiy, *Fusion Materials Semiannual Report June. 30, 2014*,. DOE/ER-0313/56 (2014) 217.